Evaluation of New Aminoalkoxide Precursors for Atomic Layer Deposition. Growth of Zirconium Dioxide Thin Films and Reaction Mechanism Studies

Raija Matero,*,† Mikko Ritala,† Markku Leskelä,† Timo Sajavaara,‡ Anthony C. Jones,§,|| and John L. Roberts§

Laboratory of Inorganic Chemistry, Department of Chemistry, P.O. Box 55, and Accelerator Laboratory, P.O. Box 43, FIN-00014, University of Helsinki, Helsinki, Finland, Department of Chemistry, University of Liverpool, Liverpool L69 3ZD, U.K., and Epichem Oxides and Nitrides, Power Road, Bromborough, Wirral, Merseyside CH62 3QF, U.K.

Received November 26, 2003. Revised Manuscript Received July 21, 2004

Atomic layer deposition (ALD) was used for growing zirconium dioxide (ZrO_2) thin films by alternate surface reactions between new aminoalkoxides and water. The zirconium aminoalkoxide precursors were $Zr(dmae)_4$, $Zr(dmae)_2(O^tBu)_2$, and $Zr(dmae)_2(O^iPr)_2$ (dmae is dimethylaminoethoxide, $[OCH_2CH_2N(CH_3)_2]$). Films were deposited on soda and borosilicate glass at 190−340 °C. The growth rate increased with elongated Zr precursor pulse possibly due to precursor decomposition. The as-deposited films contained substantial amounts of residual hydrogen. Reaction mechanisms were studied with a quadrupole mass spectrometer (QMS) and a quartz crystal microbalance (QCM) connected to the ALD reactor. The QMS results showed that the precursors decompose at higher temperatures, $Zr(dmae)_4$ making an exception. According to the QCM results, all precursors start to decompose with longer Zr precursor pulses.

1. Introduction

Zirconium dioxide (ZrO_2) has been studied extensively in searching for new high-*k* gate dielectric materials for CMOS devices.[1−4] Atomic layer deposition (ALD) is a promising method for deposition of ZrO_2 films for various purposes, as under properly chosen reaction conditions highly conformal and uniform films are obtained.[5,6] The film thickness can be controlled precisely by the number of reaction cycles repeated.

In the ALD of ZrO_2, halides and some organic and organometallic compounds have been used as the zirconium precursor: $ZrCl_4$,[7−11] ZrI_4,[12] $Zr(O^tBu)_4$,[13] $Zr(NR_2)_4$,[14] $Zr(thd)_4$,[15] $Zr(acac)_4$,[16] $Zr(butylacetoacetate)_4$,[16] $Cp_2Zr(CH_3)_2$,[15] and Cp_2ZrCl_2.[15] The oxygen sources have been H_2O,[7,12−14] H_2O_2,[12] O_2,[16] and O_3.[15] $ZrCl_4$ has so far been the most commonly used precursor. As it is a solid source, there is a risk of particle transportation onto the substrates. It also leaves some chlorine residue in the films. Simple alkoxides, such as $Zr(O^tBu)_4$, suffer from poor thermal stability.[13] We previously examined $Zr(dmae)_2(O^tBu)_2$ (dmae = $[OCH_2CH_2N(CH_3)_2]$) and H_2O as an alternative process.[17,18] In $Zr(dmae)_2(O^tBu)_2$, the coordination number of Zr has been increased by incorporating a donor-functionalized alkoxo ligand in an attempt to stabilize the molecule. However, only a limited success was achieved in ALD, probably because of the two easily decomposing $-O^tBu$ ligands.

In this work, ZrO_2 thin films were deposited using aminoalkoxide compounds $Zr(dmae)_4$ and $Zr(dmae)_2(O^iPr)_2$. These precursors are compared to $Zr(dmae)_2(O^tBu)_2$, and new results concerning that precursor are

* To whom correspondence should be addressed.
† Department of Chemistry, University of Helsinki.
‡ Accelerator Laboratory, University of Helsinki.
§ University of Liverpool.
|| Epichem Oxides and Nitrides.

(1) Tsai, W.; Carter, R. J.; Nohira, H.; Caymax, M.; Conard, T.; Cosnier, V.; DeGendt, S.; Heyns, M.; Petry, J.; Richard, O.; Vandervorst, W.; Young, E.; Zhao, C.; Maes, J.; Tuominen, M.; Schulte, W. H.; Garfunkel, E.; Gustafsson, T. *Microelectron. Eng.* **2003**, *65*, 259.
(2) Perkins, C. M.; Triplett, B. B.; McIntyre, P. C.; Saraswat, K. C.; Haukka, S.; Tuominen, M. *Appl. Phys. Lett.* **2001**, *78*, 2357.
(3) Copel, M.; Gribelyuk, M.; Gusev, E. *Appl. Phys. Lett.* **2000**, *76*, 436.
(4) Lee, D.-O.; Roman, P.; Wu, C.-T.; Mumbauer, P.; Brubaker, M.; Grant, R.; Ruzyllo *J. Solid-State Electron.* **2002**, *46*, 1671.
(5) Suntola, T. *Thin Solid Films* **1992**, *216*, 84.
(6) Ritala, M.; Leskelä, M. In *Handbook of Thin Film Materials*; Nalwa, H. S., Ed.; Academic: San Diego; 2001; Vol. 1, Chapter 2, p 103.
(7) Ritala, M.; Leskelä, M. *Appl. Surf. Sci.* **1994**, *75*, 333.
(8) Ferrari, S.; Dekadjevi, D. T.; Spiga, S.; Tallarida, G.; Wiemer, C.; Fanciulli, M. *J. Non-Cryst. Solids* **2002**, *303*, 29.
(9) Zhao, C.; Roebben, G.; Bender, H.; Young, E.; Haukka, S.; Houssa, M.; Naili, M.; De Gendt, S.; Heyns, M.; Van Der Biest, O. *Microelectron. Reliab.* **2001**, *41*, 995.
(10) Aarik, J.; Aidla, A.; Mändar, H.; Uustare, T.; Sammelselg, V. *Thin Solid Films* **2002**, *408*, 97.
(11) Rahtu, A.; Ritala, M. *J. Mater. Chem.* **2002**, *12*, 1484.
(12) Kukli, K.; Forsgren, K.; Aarik, J.; Aidla, A.; Uustare, T.; Ritala, M.; Niskanen, A.; Leskelä, M.; Hårsta, A. *J. Cryst. Growth* **2001**, *231*, 262.
(13) Kukli, K.; Ritala, M.; Leskelä, M. *Chem. Vap. Deposition* **2000**, *6*, 297.
(14) Hausmann, D. M.; Kim, E.; Becker, J.; Gordon, R. G. *Chem. Mater.* **2002**, *14*, 4350.
(15) Putkonen, M.; Niinistö, L. *J. Mater. Chem.* **2001**, *11*, 3141.
(16) Chakraborty, A.; Mane, A. U.; Shivashankar, S. A.; Venkataraman, V. *Mater. Res. Soc. Symp. Proc.* **2003**, *745*, 143.
(17) Matero, R.; Ritala, M.; Leskelä, M.; Jones, A. C.; Williams, P. A.; Bickley, J. F.; Steiner, A.; Leedham, T. J.; Davies, H. O. *J. Non-Cryst. Solids* **2002**, *303*, 24.
(18) Jones, A. C.; Williams, P. A.; Roberts, J. L.; Leedham, T. J.; Davies, H. O.; Matero, R.; Ritala, M.; Leskelä, M. *Mater. Res. Soc. Symp. Proc.* **2002**, *716*, 145.

10.1021/cm030669f CCC: $27.50
Published on Web 11/20/2004

also presented. The film growth has been studied in situ by a quadrupole mass spectrometer (QMS) and a quartz crystal microbalance (QCM).

2. Experimental Section

2.1. Precursor Synthesis. $Zr(dmae)_2(O^iPr)_2$ was synthesized by the dropwise addition of dmaeH ($HOCH_2CH_2NMe_2$) (9.4 cm^3, 17.1 g, 192.5 mmol) to $Zr(O^iPr)_4$ (37.3 g, 96.2 mmol) in hexane (200 mL). The solution was heated under reflux for 1 h. The volatiles were then removed under reduced pressure, and the product was recrystallized from pentane at 5 °C, to give colorless needles. Yield: 32.1 g (87% based on $Zr(O^iPr)_4$).

Anal. Calcd: C: 43.4, H: 8.8, N: 7.2. Found: C: 41.4, H: 8.9, N: 7.5.

The deviation of the carbon value found from the expected value may indicate the presence of a small amount of impurity.

^1H NMR (400 MHz, C_6D_6, ppm): 1.60 (s, CC*H*$_3$, 12H), 2.42 (s, NC*H*$_3$, 12H), 2.74 (s, CH_2, 4H), 4.36 (s, CH_2, 4H), 4.77 (s, CH, 2H).

The proton NMR data showed clear evidence of exchange of alkoxide groups, which leads to a significant broadening of resonances so that all appeared as very broad singlets. Alkoxide exchange is a common feature of zirconium alkoxide chemistry, and very similar NMR data have already been reported for the related complexes $[Zr(O^iPr)_3(bis\text{-}dmap)]_2$ and $[Zr(O^iPr)_3(dmap)]_2$ (dmap = $OCHMeCH_2NMe_2$; bis-dmap = $OCH(CH_2NMe_2)_2$).[19a]

$Zr(dmae)_4$ was synthesized by the dropwise addition of dmaeH (4 mol equiv) to $Zr(NEt_2)_4$ in toluene. The solution was heated under reflux for 1 h, and then volatiles were removed in vacuo to leave the product as a viscous oil which had ^1H NMR data identical to published values.[19b]

2.2. Film Growth and Characterization. The films were grown on 5 cm × 5 cm soda lime and borosilicate glass substrates at temperatures between 190 and 340 °C in a hot-wall flow-type F-120 ALD reactor manufactured by ASM Microchemistry Ltd. Nitrogen (99.999%) was used as a precursor carrier and purge gas. The pressure in the reactor was about 10 mbar. The Zr precursors were evaporated from an open boat inside the reactor. The evaporation temperatures were 150 °C for $Zr(dmae)_2(O^iPr)_2$ and $Zr(dmae)_2(O^tBu)_2$ and 170 °C for $Zr(dmae)_4$. Water was held in an external reservoir at room temperature and led into the reactor through needle and solenoid valves. Thicknesses and refractive indices of the films were evaluated by fitting transmittance spectra according to the method developed and described by Ylilammi and Ranta-aho.[20] The transmittance spectra were measured within a wavelength region of 380−1100 nm by a Hitachi U-2000 spectrophotometer. The refractive indices are given for $\lambda = 580$ nm. The crystal structure and orientation of the films were studied by a Philips MPD 1880 powder XRD diffractometer using Cu Kα radiation. The chemical composition of the films was examined by time-of-flight elastic recoil detection analysis (TOF-ERDA) using a 53 MeV $^{127}I^{6+}$ beam obtained from a 5 MV tandem accelerator, EPG-10-II, at the Accelerator Laboratory.[21]

2.3. Reaction Mechanism Studies. The QMS−QCM−ALD experiments were made in a commercial flow-type ALD reactor manufactured by ASM Microchemistry Ltd., specially modified in-house for in situ studies. The equipment has been described in detail elsewhere.[22] The gas composition was measured with a Hiden HAL/3F 501 RC QMS, which has a mass range of 1−510 amu. A Faraday cup detector was used; the ionization energy was 70 eV. The pressure in the ALD reaction chamber was about 2 mbar, and it was reduced to about 10^{-7} mbar in the QMS chamber by differential pumping through an orifice of 200 μm in diameter. The mass balance studies were done using a Maxtek TM 400 QCM. The operating frequency of the crystal was 6 MHz; the sampling rate was 20 times/s.

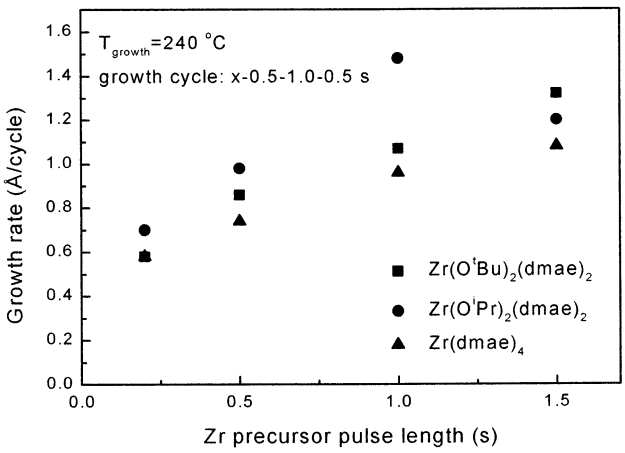

Figure 1. Growth rates of ZrO_2 films presented as a function of the Zr precursor pulse length. The inset shows the pulsing sequence and the growth temperature.

The growth temperatures and the evaporation temperatures of the precursors were the same as in the film growth experiments. D_2O (Euriso-top, 99.9% D) was used as the oxygen source instead of H_2O to distinguish the species coming from the surface reactions from those coming directly from the precursor.

The following pulsing sequence was used: 5 times D_2O pulse/purge, 10 times Zr precursor pulse/purge/D_2O pulse/purge, 5 times Zr precursor pulse/purge. A 10 s D_2O pulse was applied before each experiment except those where the precursor decomposition was studied. In the case of the QMS measurements, the background signals (measured during the first five successive D_2O pulses and the five successive Zr precursor pulses in the end) arising from precursor decomposition and fragmentation were subtracted from the data measured during the ALD process. The D_2O and Zr precursor pulse lengths were varied between 1 and 7.0 s.

3. Results and Discussion

3.1. Film Growth. The length of the Zr precursor pulse was varied between 0.2 and 1.5 s using a 1.0 s water pulse. Figure 1 presents growth rates as a function of Zr precursor pulse length. It can be seen that the growth rate increases steadily when the precursor pulse is elongated and no saturation of the surface is achieved. This was first attributed to decomposition of the organometallic precursor on the surface. In our previous study,[17] this assumption was tested by pulsing only $Zr(dmae)_2(O^tBu)_2$ on ZrO_2 films and bare glass substrates. No or barely any film was obtained at 240 °C using a 0.2 s pulse. This was found to be the case also in this study with $Zr(dmae)_2(O^iPr)_2$ and $Zr(dmae)_4$ at 240 °C. $Zr(dmae)_2(O^iPr)_2$ was examined also at 340 °C and with a 1.5 s pulse: no film was deposited. This suggests that the decomposition of the precursor may be induced by the surface OH groups that are formed in exchange reactions with water. The repeatedly incoming water pulses maintain high −OH coverage on the surface and thereby enhance the decomposition.

The role of the surface OH groups with respect to the metal precursor decomposition has been considered also

(19) (a) Fleeting, K. A.; O'Brien, P.; Jones, A. C.; Otway, D. J.; White, A. J. P.; Williams, D. J. *J. Chem. Soc., Dalton Trans.* **1999**, 2853. (b) Na, J. S.; Kim, D.-H.; Yong, K.; Rhee, S.-W. *J. Electrochem. Soc.* **2002**, *149*, C23.

(20) Ylilammi, M.; Ranta-aho, T. *Thin Solid Films* **1993**, *232*, 56.

(21) Jokinen, J.; Haussalo, P.; Keinonen, J.; Ritala, M.; Riihelä, D.; Leskelä, M. *Thin Solid Films* **1996**, *289*, 159.

(22) Rahtu, A.; Ritala, M. *Electrochem. Soc. Proc.* **2000**, *2000−13*, 105.

by Cameron and George,[23] who suggested a mechanism for the heterogeneous decomposition of $Zr(O^tBu)_4$. In reactions 1−6 "s" denotes a surface-bound species. $Zr(O^tBu)_4$ becomes bound to the surface by reacting with a hydroxyl group. In this reaction a *tert*-butoxide ligand is eliminated as *tert*-butyl alcohol.

$$-(OH)(s) + Zr(O^tBu)_4 \rightarrow -O-Zr(O^tBu)_3(s) + Bu^tOH \quad (1)$$

The remaining $-O^tBu$ groups may decompose by β-hydride elimination, producing isobutylene and creating new OH groups on the surface.

$$Zr-(O^tBu)(s) \rightarrow Zr-(OH)(s) + CH_2C(CH_3)_2 \quad (2)$$

The same kind of reaction has been proposed for $Ti(O^iPr)_4$,[24] though it has also been suggested that the ligands could be eliminated from the surface by reacting with another nearby ligand or with some other nucleophilic surface group, particularly hydroxide or oxide ions.[25] The mechanism could be applied to $Zr(O^iPr)_4$ as well. In reactions on a −OH-covered surface, propanol is produced and the ligands remaining on the surface may decompose, creating propene and new −OH surface groups.

$$-(OH)(s) + Zr(O^iPr)_4 \rightarrow -O-Zr(O^iPr)_3(s) + Pr^iOH \quad (3)$$

$$Zr-(O^iPr)(s) \rightarrow Zr-(OH)(s) + CH_2CHCH_3 \quad (4)$$

The decomposition mechanism of the surface-bound dmae ligand is apparently similar.

$$-(OH)(s) + Zr[OCH_2CH_2N(CH_3)_2]_4 \rightarrow -O-Zr[OCH_2CH_2N(CH_3)_2]_3(s) + (CH_3)_2NCH_2CH_2OH \quad (5)$$

$$Zr-[OCH_2CH_2N(CH_3)_2](s) \rightarrow Zr-(OH)(s) + CH_2CHN(CH_3)_2 \quad (6)$$

Figure 1 also depicts the effect of the ligands attached to Zr on the growth rate: the lowest values are obtained with $Zr(dmae)_4$ and the highest with $Zr(dmae)_2(O^iPr)_2$. The growth rates we obtained earlier when using $Zr(dmae)_2(O^tBu)_2$[17] place themselves between those values. Overall, the growth rates vary between 0.58 and 1.48 Å/cycle. These are somewhat higher than those obtained using halide precursors: 0.53 Å/cycle (at 500 °C) with $ZrCl_4$[7] and 0.4−1.25 Å/cycle with ZrI_4 (at 250−350 °C).[12] With $Zr(O^tBu)_4$[13] growth rates from 0.5 to 6.5 Å/cycle were obtained when the $Zr(O^tBu)_4$ pulse length was varied from 0.2 to 1.5 s. The very high growth rates were attributed to self-decomposition of the *tert*-butoxide group. The growth rate lowering factor in our study compared to $Zr(O^tBu)_4$ must be the dmae ligand.

The effect of the H_2O pulse length on the growth rate is shown in Figure 2. Pulse length variation between 0.2 and 1.5 s does not have a large effect. The growth rate seems to saturate with a 1.0 s water pulse, which therefore appears to be the optimum pulse length. Kukli et al.[13] obtained similar results in their study with $Zr(O^tBu)_4$: the water pulse length had a minimal effect on the film growth rate. Figure 3 shows that the growth temperature had only a minor effect when a short (0.2 s) Zr precursor pulse was used: the growth rates are quite constant over the whole temperature range (190−340 °C) regardless of the precursor used. $Zr(dmae)_4$ makes an exception: at 190 °C only a very thin film was obtained, possibly because of slow reactions at this low temperature. The weak dependence of the growth rate on temperature is quite surprising considering that precursor decomposition seems to be involved. This could be explained, though, by the fact that short 0.2 s Zr precursor pulses were used.

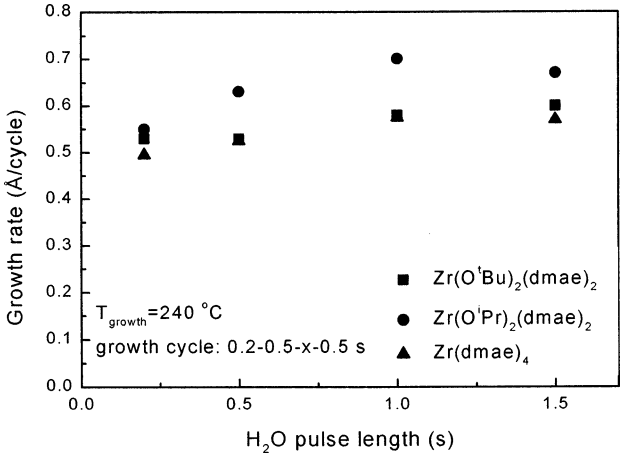

Figure 2. Growth rates of ZrO_2 films as a function of H_2O pulse length.

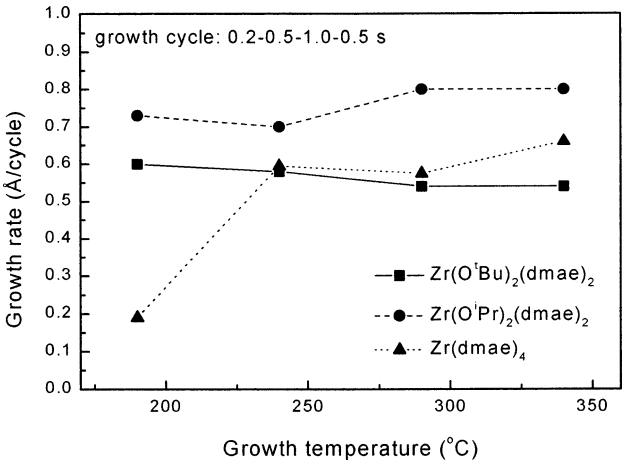

Figure 3. Growth rates of ZrO_2 films as a function of the growth temperature. The lines are only to guide the eye.

3.2. Film Characterization. It was shown earlier with $Zr(dmae)_2(O^tBu)_2$ that the refractive indices of the films vary depending on the growth parameters.[17] The same goes for the other two Zr precursors too. When the Zr precursor pulse was elongated, the refractive index decreased. Varying the water pulse length at 240 °C (a 0.2 s Zr pulse), the highest refractive indices were evaluated for the films grown using the 1.0 s pulse regardless of the Zr precursor used. The refractive index increased with increasing deposition temperature; the highest values were observed in the films grown at 340 °C: 2.0 for $Zr(dmae)_4$, 2.1 for $Zr(dmae)_2(O^iPr)_2$, and 2.0

(23) Cameron, M. A.; George, S. M. *Thin Solid Films* **1999**, *348*, 90.

(24) Chen, S.; Mason, M. G.; Gysling, H. J.; Paz-Pujalt, G. R.; Blanton, T. N.; Castro, T.; Chen, K. M.; Fictorie, C. P.; Gladfelter, W. L.; Franciosi, A.; Cohen, P. I. *J. Vac. Sci. Technol., A* **1993**, *11*, 2419.

(25) Fictorie, C. P.; Evans, J. F.; Gladfelter, W. L. *J. Vac. Sci. Technol., A* **1994**, *12*, 1108.

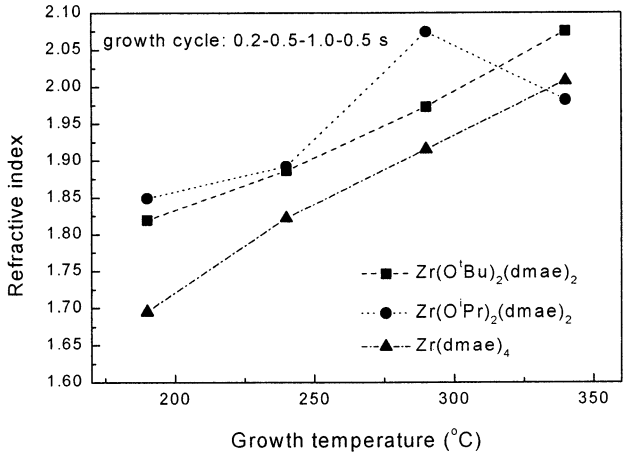

Figure 4. Refractive index of ZrO_2 films at different growth temperatures. The lines are only to guide the eye.

for $Zr(dmae)_2(O^tBu)_2$ (Figure 4). The refractive indices measured for the films grown earlier using $Zr(O^tBu)_4$[13] did not exceed 2.0. Higher values have been presented for the films grown from the halides: 2.2 for $ZrCl_4$[7] and 2.23 for ZrI_4.[12] The refractive indices of our films were improved by thermal annealing. For example, when films grown at 240 °C were annealed at 500 °C for 1 h, the refractive indices were improved from 1.9 to 2.1 [$Zr(dmae)_2(O^tBu)_2$ and $Zr(dmae)_2(O^iPr)_2$] and from 1.8 to 2.0 [$Zr(dmae)_4$]. Annealing did not noticeably improve the refractive index of the films deposited at 340 °C, however. In general, a high refractive index refers to a dense film structure.[26] Therefore, the increase in the refractive index during annealing refers to densification of the film material, which is strongly supported by the observed 30−40% thickness decrease of the films. Annealing did not affect the thickness of the films grown at 340 °C.

The films grown at 240 °C (Figure 5a) are fairly uniform; the thickness difference between the leading and the trailing edge of the substrate is about 7% for $Zr(dmae)_2(O^tBu)_2$ and $Zr(dmae)_2(O^iPr)_2$ and only about 2% for $Zr(dmae)_4$. The film uniformities are high considering the precursor decomposition which thereby needs to proceed under surface reaction rate control. One should take into account that very short 0.2 s Zr precursor pulses were used. In the films grown at 340 °C (Figure 5b) there is a larger thickness deviation: about 30% for $Zr(dmae)_2(O^tBu)_2$ and $Zr(dmae)_2(O^iPr)_2$ and about 13% for $Zr(dmae)_4$.

The chemical composition of the films was analyzed by TOF-ERDA. Because a large part of the hydrogen and carbon left the as-deposited films during analysis, accurate amounts could not be determined. Therefore, the results should only be considered as qualitative. Anyhow, the films deposited at 240 °C using 0.2 s Zr precursor pulses contained considerable amounts of hydrogen: at least 30 atom % for $Zr(dmae)_4$ and at least 12 atom % for $Zr(dmae)_2(O^tBu)_2$. No value could be determined for the films grown from $Zr(dmae)_2(O^iPr)_2$. Elongating the Zr precursor pulse did not affect the hydrogen content. In the case of $Zr(dmae)_4$, elongating the H_2O pulse to 1.5 s produced films with only about 9

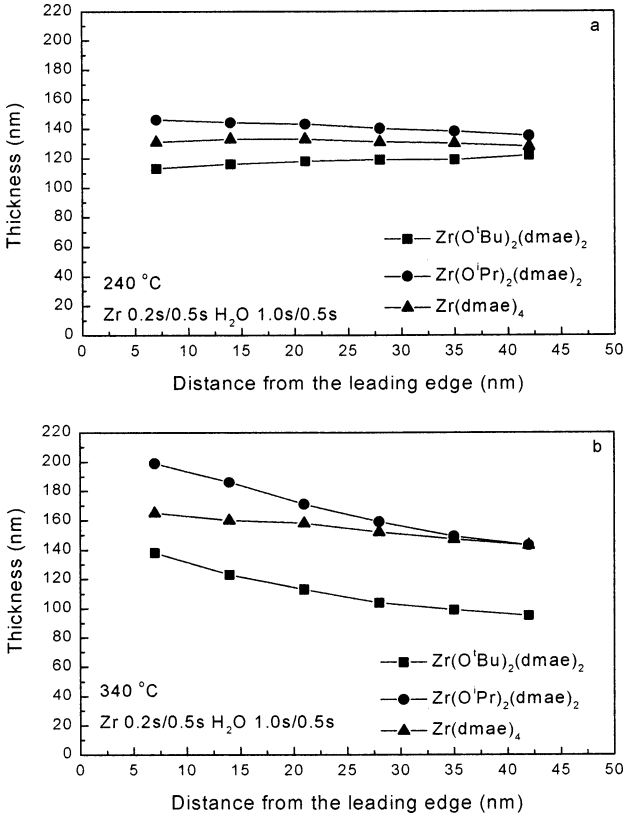

Figure 5. Film thickness determined at six points starting from the leading edge. The inset shows the pulsing sequence. The film growth temperature is (a) 240 °C and (b) 340 °C.

atom % hydrogen. The carbon content is the largest in the films grown using $Zr(dmae)_4$, at least 5 atom %. Elongating the Zr precursor or water pulse does not have an effect on the carbon content regardless of the Zr precursor. There is also a small nitrogen residue in all the films, in most cases less than 1 atom %, but a maximum of 4 atom % is found in the film grown using a 1.5 s $Zr(dmae)_4$ pulse. In the films grown at 340 °C, smaller amounts of impurities were detected; for example, the hydrogen content is about half that in the films grown at 240 °C. The impurity contents of the annealed (500 °C) films were significantly lower, as we assumed earlier.[17] This assumption is also supported by the improved refractive index. At this point, it is hard to say whether the origin of the hydrogen is H_2O or the Zr compound.

The crystallinity of the films was examined by XRD. We have previously presented results concerning the films grown from $Zr(dmae)_2(O^tBu)_2$.[17] The films grown at 190−240 °C were amorphous as no peaks were detected by XRD. In the films grown at 290−340 °C a broad peak was detected at $2\theta = 35.4°$. In the films grown at 340 °C an additional broad peak of low intensity was detected at 30.5° (Figure 6). In the films grown using $Zr(dmae)_2(O^tBu)_2$ and $Zr(dmae)_2(O^iPr)_2$ yet another peak of very low intensity can be seen at 51.0° (Figure 6). As the peaks were wide and their intensity was low, it was not possible to determine the ZrO_2 phase reliably, i.e., whether they had monoclinic, tetragonal, or cubic structure. Thermal annealing for 1 h under N_2 at 500 °C turned the as-deposited amorphous films into nanocrystalline films: a clear peak appeared at 30.5° and peaks of low intensity at 35.4°, 51.0°, and 60.5°.

(26) Otterman, C. R.; Bange, K.; Wagner, W.; Laube, M.; Rauch, F. *Surf. Interface Anal.* **1992**, *19*, 435.

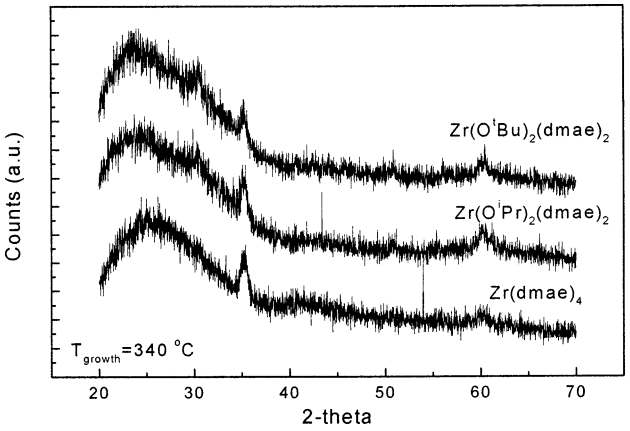

Figure 6. XRD diffractograms for as-deposited films grown at 340 °C.

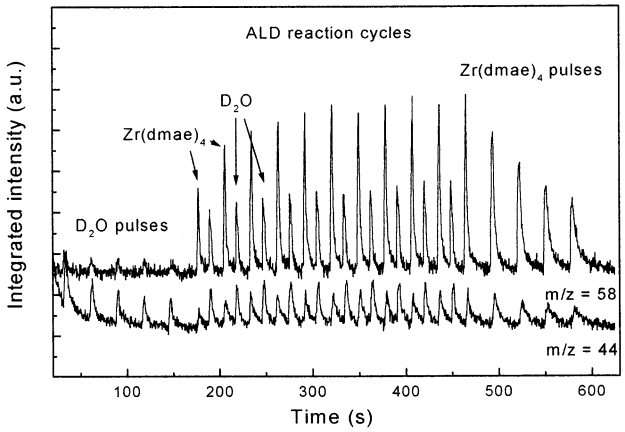

Figure 7. QMS data recorded for the Zr(dmae)$_4$−D$_2$O process at 240 °C. The data have been shifted vertically for clarity.

When the nanocrystalline films that were deposited at 340 °C were annealed at 500 °C, the only change was that the peak at 30.5° became more visible.

3.3. Growth Mechanism. As the reaction mechanism studies were carried out in an ALD reactor with a larger reaction chamber than that used in the film growth experiments, longer pulse times were needed; 3.0 s pulses were used unless otherwise stated. The long pulse times obviously have an emphasizing effect on the precursor decomposition.

Ideal ALD growth would proceed solely via ligand exchange reactions on the film surface. When Zr(dmae)$_4$ and water, for example, are pulsed alternately onto the substrates, the following reactions should occur (the number of −OD groups, and hence the number of dmae ligands that react during the Zr(dmae)$_4$ pulse, varies according to the reaction conditions, particularly temperature). In reactions 7−14 "s" denotes surface species and "g" species in the gas phase.

$$2\ {-}OD(s) + Zr(dmae)_4(g) \rightarrow (-O-)_2Zr(dmae)_2(s) + 2dmaeD(g) \quad (7)$$

$$(-O-)_2Zr(dmae)_2(s) + 2D_2O(g) \rightarrow (-O-)_2Zr(OD)_2(s) + 2dmaeD(g) \quad (8)$$

The main reaction byproduct should be dmaeD, but we observed hardly any $m/z = 90$ $[dmaeD]^+$ with the QMS. It is most probably fragmented, the main fragment being $m/z = 58$ $[CH_2N(CH_3)_2]^+$, which is produced by α-cleavage and was found in significant amounts. Another fragment produced by the α-cleavage would be $m/z = 32$ $[DOCH_2]^+$, but we obtained only a very weak signal at $m/z = 32$ as the formation of $m/z = 58$ is more favorable. We also observed $m/z = 44$ $[CH_2NHCH_3]^+$, which is produced by a secondary rearrangement reaction. Figure 7 shows QMS data of $m/z = 58$ and 44. Both ions are produced during both the Zr(dmae)$_4$ pulse and the D$_2$O pulse. The amount of these ions decreased slightly with increasing growth temperature.

When two different ligands are attached to Zr, the situation is more complicated as there are two possible reaction byproducts and combinations of those during each precursor pulse. Reactions 9−14 give an example of possible reactions when the incoming Zr precursor reacts with two −OD groups, −OR = −O^{t}Bu, −O^{i}Pr. Again, the number of −OD groups with which the metal precursor reacts depends on the reaction conditions.

$$2\ {-}OD(s) + Zr(dmae)_2(OR)_2(g) \rightarrow (-O-)_2Zr(OR)_2\ (s) + 2dmaeD(g) \quad (9)$$

$$(-O-)_2Zr(OR)_2(s) + 2D_2O(g) \rightarrow (-O-)_2Zr(OD)_2(s) + 2ROD(g) \quad (10)$$

$$2\ {-}OD(s) + Zr(dmae)_2(OR)_2(g) \rightarrow (-O-)_2Zr(dmae)_2(s) + 2ROD(g) \quad (11)$$

$$(-O-)_2Zr(dmae)_2(s) + 2D_2O(g) \rightarrow (-O-)_2Zr(OD)_2(s) + 2dmaeD(g) \quad (12)$$

$$2\ {-}OD(s) + Zr(dmae)_2(OR)_2(g) \rightarrow (-O-)_2Zr(dmae)(OR)(s) + dmaeD(g) + ROD(g) \quad (13)$$

$$(-O-)_2Zr(dmae)(OR)(s) + 2D_2O(g) \rightarrow (-O-)_2Zr(OD)_2(s) + dmaeD(g) + ROD(g) \quad (14)$$

The main reaction byproducts in the case of Zr(dmae)$_2$(O^{t}Bu)$_2$ should be dmaeD and Bu^{t}OD ($m/z = 75$), which, however, were not observed with the QMS, but again fragments at $m/z = 58$ $[CH_2N(CH_3)_2]^+$ and $m/z = 60$ $[(CH_3)_2COD]^+$ were found. The mass $m/z = 60$ is detected also from Zr(dmae)$_2$(O^{i}Pr)$_2$ and Zr(dmae)$_4$, but the amounts are much smaller. In the case of Zr(dmae)$_2$(O^{i}Pr)$_2$, a fragment $[CH_3CHOD]^+$ of the expected main byproduct Pr^{i}OD was observed at $m/z = 46$. This mass was also observed from the other two precursors, but the amounts were very small compared to that for Zr(dmae)$_2$(O^{i}Pr)$_2$. Interestingly, with Zr(dmae)$_2$(O^{i}Pr)$_2$ most of the $m/z = 46$ is observed during the Zr pulse, but with the other two precursors it is mostly observed during the D$_2$O pulse. Similar to Zr(dmae)$_2$(O^{t}Bu)$_2$, the expected main byproduct coming from the dmae ligand, $m/z = 90$, was not detected from Zr(dmae)$_2$(O^{i}Pr)$_2$. The fragments $m/z = 58$ and $m/z = 44$ were observed, however, but in contrast to Zr(dmae)$_4$, the amounts of these ions now increased with increasing temperature. This suggests that part of the detected ions at $m/z = 58$ and $m/z = 44$ are coming from the other two ligands, −O^{t}Bu and −O^{i}Pr ($m/z = 58$ $[(CH_3)_2CO]^+$ and $m/z = 44$ $[CH_3CHO]^+$), either directly or indirectly.

Table 1. Studied *m/z* Values and the Suggested Corresponding Ions and Whether They Were Detected or Not

m/z	ion	Zr(dmae)	$Zr(dmae)_2(O^tBu)_2$	$Zr(dmae)_2(O^iPr)_2$
31	$[CH_2OH]^+$	yes	yes	yes
41	$[CH_3CCH_2]^+$	yes	yes	yes
	$[CHNCH_2]^+$			
42	$[CH_2CHCH_3]^+$	yes	yes	yes
	$[CH_2NCH_2]^+$			
43	$[CH_2COH]^+$	yes	yes	yes
	$[CH_2NCH_3]^+$			
44	$[CH_3CHO]^+$	yes	yes	yes
	$[CH_2NHCH_3]^+$			
46	$[CH_3CHOD]^+$	yes	yes[a]	yes
	$[DOCH_2CH_2]^+$			
56	$[CH_2C(CH_3)_2]^+$	yes	yes	yes
	$[C_3H_6N]^+$			
58	$[CH_2N(CH_3)_2]^+$	yes	yes	yes
	$[(CH_3)_2CO]^+$			
59	$[(CH_3)_2CHO]^+$	yes	yes	yes
	$[(CH_3)_3N]^+$			
60	$[(CH_3)_2COD]^+$	yes[a]	yes	yes
	$[(CH_3)_2NCH_2D]^+$			
71	$[CH_2CHN(CH_3)_2]^+$	yes	yes	yes
74	$[(CH_3)_2COH]^+$	no	no	no
75	$[(CH_3)_3COD]^+$	no	no	no
88	$[(CH_3)_2NCH_2CH_2O]^+$	no	no	no
89	$[(CH_3)_2NCH_2CH_2OH]^+$	yes	no	no
90	$[(CH_3)_2NCH_2CH_2OD]^+$	yes	no	no

[a] A very small amount was detected.

A list of the *m/z* values that were measured from all three precursors is presented in Table 1. The mass *m/z* = 31 $[CH_2OH]^+$ is formed by α-cleavage of the dmaeH ligand, but it is also produced by thermal decomposition of the other two ligands, as the amounts observed during the Zr precursor pulses increase with increasing temperature when $Zr(dmae)_2(O^tBu)_2$ and $Zr(dmae)_2(O^iPr)_2$ are used. The amounts of the masses *m/z* = 41 and *m/z* = 43 also increase on going from 240 to 340 °C with $Zr(dmae)_4$. Those masses were measured from the other two precursors only at 240 °C. It can be seen from Table 1 that we were not able to find a mass coming from any of the precursors exclusively; therefore, we were not able to deduce detailed reaction mechanisms at different temperatures, i.e., how many and which ligands are eliminated during the Zr precursor pulses and which ones during the water pulses.

One mechanism for the decomposition was suggested by reactions 1−6. The alcohols formed in reactions 1 and 5 (*m/z* = 74 and *m/z* = 89) were not observed. The propanol formed in reaction 3 would be at *m/z* = 60, which was detected with all three precursors, so we are not able to conclude whether it presents propanol or some other ion with the same mass. The masses *m/z* = 42 $[CH_2CHCH_3]^+$, *m/z* = 56 $[CH_2C(CH_3)_2]^+$, and *m/z* = 71 $[CH_2CHN(CH_3)_2]^+$ were detected for all three precursors; however, the amount of *m/z* = 42 was larger when $Zr(dmae)_2(O^iPr)_2$ was involved, and correspondingly *m/z* = 56 when $Zr(dmae)_2(O^tBu)_2$ was involved. This suggests that reactions 2 and 3 might take place. No conclusions can be drawn concerning reaction 5 as the mass *m/z* = 71 was checked from all three precursors only at 340 °C.

Decomposition of the precursors obviously leads to a complicated overall reaction mechanism. Especially at the higher growth temperatures decomposition plays a big role. This can be seen in Figure 8, for example, which shows that the background signals coming from the Zr precursors are quite strongly dependent on temperature. In the absence of decomposition they should stay more constant. At 340 °C the background signal exceeds the amount of the same mass (*m/z* = 58) detected during the ALD reactions. The extensive decomposition is seen in the data concerning $Zr(O^tBu)_2(dmae)_2$ and $Zr(O^iPr)_2(dmae)_2$, but the $Zr(dmae)_4$ data show a weaker dependence on temperature. A similar behavior was seen, for example, with the mass *m/z* = 44.

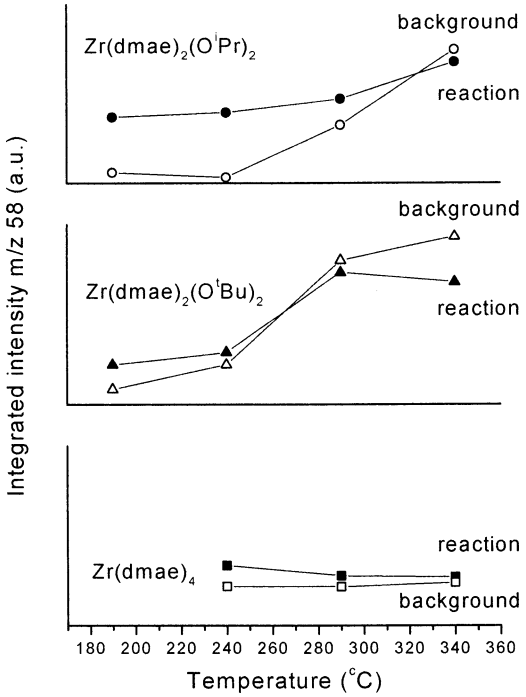

Figure 8. Amount of *m/z* 58 measured with the QMS at 240 °C (reaction, the amount detected during ALD reaction; background, the amount coming from the Zr precursor).

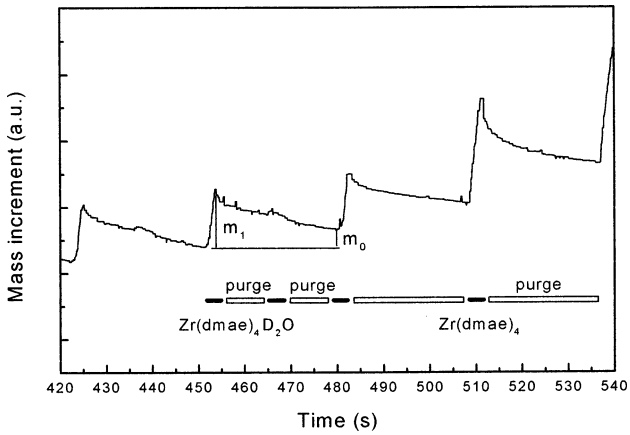

Figure 9. QCM mass change during two $Zr(dmae)_4$−D_2O ALD cycles and two $Zr(dmae)_4$ pulses at 240 °C.

At the same time as the QMS measurements, the film growth was monitored with a QCM. Decomposition of the precursors can also be seen in the QCM data. Part of the signal recorded at 240 °C is presented in Figure 9. The mass increases without saturation during the Zr precursor pulse and then decreases rapidly during the following purge. This indicates clearly that the precursor decomposes. The mass increases also during the Zr precursor background pulses, which further confirms decomposition. The data were similar for all three precursors.

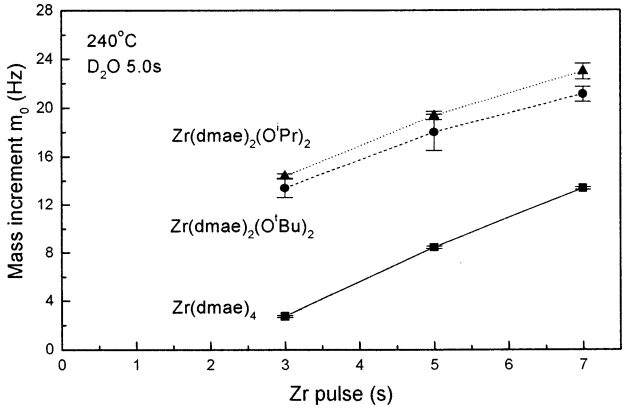

Figure 10. m_0 determined from data recorded with different Zr precursor pulse lengths. The line is only to guide the eye.

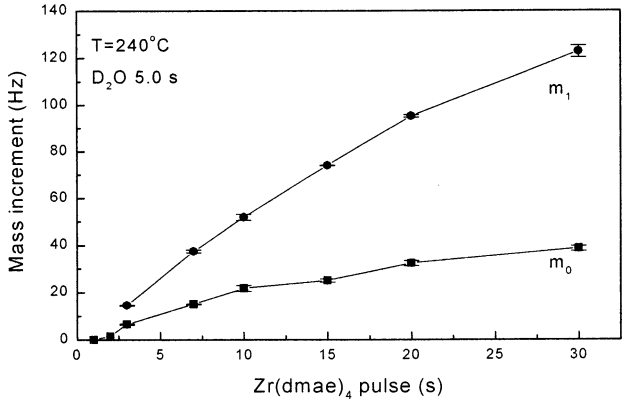

Figure 11. m_0 determined with elongated $Zr(dmae)_4$ pulses at 240 °C.

The mass increment during one ALD cycle, m_0, increases when the Zr precursor pulse is elongated (Figure 10). No saturation is achieved, not even with very long pulses. Figure 11 shows the obtained m_0 and m_1 values, the latter being the mass increment during the metal pulse, when the $Zr(dmae)_4$ pulse was elongated to 30 s at 240 °C. Because of the decomposition, both values increase without saturation.

The decomposition was also studied by pulsing only the Zr precursor onto the substrates. The QCM showed that $Zr(dmae)_2(O^tBu)_2$ decomposes at 190−340 °C even when no water is applied. During the first couple of pulses, the mass increment is larger than during the rest of the pulsing sequence (Figure 12). Similar results were obtained with $Zr(dmae)_2(O^iPr)_2$ and $Zr(dmae)_4$. At this stage, the precursors most probably react according to reactions 1, 3, and 5 slowly, consuming the surface

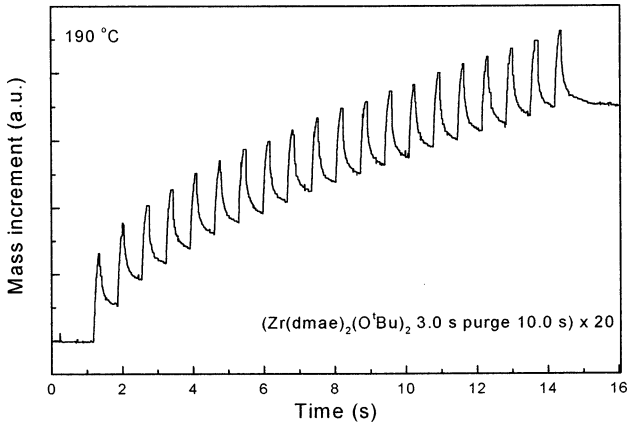

Figure 12. QCM data that were collected while only $Zr(dmae)_2(O^tBu)_2$ was pulsed on the ZrO_2 surface at 190 °C.

OH groups. This observation supports our suggestion of the decomposition-enhancing effect of high hydroxyl coverage. During the rest of the pulses, the mass increment settles to a certain level, which suggests that the ligands decompose by creating new surface sites according to reactions 2, 4, and 6. The number of these OH groups created by β-elimination is low compared to the initial OH coverage; hence, the mass increment is much smaller.

4. Conclusions

ZrO_2 films can be grown by an ALD-like process using water and new aminoalkoxide zirconium precursors, $Zr(dmae)_4$, $Zr(dmae)_2(O^tBu)_2$, and $Zr(dmae)_2(O^iPr)_2$. No saturation of the surface can be achieved, however, because of the decomposition of the precursors. There are significant amounts of residual hydrogen and carbon in the films. These impurities are probably caused by the decomposition. The impurity content can be reduced by thermal annealing. According to the QMS results, $Zr(dmae)_4$ seems to be the thermally most stable of the three precursors. The QCM results, however, show extensive decomposition at higher temperatures and with longer Zr pulses.

Acknowledgment. Dr. Antti Rahtu is acknowledged for help with the QMS and QCM measurements. This work was financially supported in part by the Finnish National Technology Agency (TEKES) and the Academy of Finland.

CM030669F